PERGAMON

International Journal of Multiphase Flow 27 (2001) 437–458

International Journal of Multiphase Flow

www.elsevier.com/locate/ijmulflow

Simulation of cluster formation in gas–solid flow induced by particle–particle collisions

E. Wassen*, Th. Frank

Research Group on Multiphase Flow, Department of Technical Thermodynamics, Chemnitz University of Technology, 09107 Chemnitz, Germany

Received 16 March 1999; received in revised form 15 March 2000

Abstract

Simulations of gas–solid flows in a horizontal channel are presented. The transient motion of the particle phase is computed using the Simultaneous Particle Tracking technique. Particle–particle collisions are accounted for by applying a Stochastic model. Particle to gas mass loading ratio is varied in the simulations from 0.01 upto 10. The influence of inter-particle collisions on the particle concentration distribution is investigated. Collisions are found to have a significant effect on the concentration distribution at moderate to high loading ratios. For high loading ratios, collisions tend to enhance the formation of particle clusters. © 2001 Elsevier Science Ltd. All rights reserved.

Keywords: Two-phase flow; Gas–solid flow; Transient simulation; Lagrangian approach; Particle–particle collision

1. Introduction

In the industrial fields of energy production and process engineering, there are many applications involving gas-particle flows, e.g. pneumatic conveying of granular material, injection of pulverized fuel into burners or separation of solid particles from flue gas. In many cases, the particle loading is moderate to high and hence particle–particle interactions significantly influence the flow behaviour. But the average loading is not the only measure for the importance of collisions. Even if the average loading in a particular application is relatively low, there may be regions of locally high concentration, e.g. in

* Corresponding author.

PII: S0301-9322(00)00028-8

"ropes" that form behind pipe bends, where collisions may have a strong macroscopic effect. Additionally, there are other factors that may increase the number and importance of collisions. For instance, near obstacles and walls the difference of velocities of impinging and rebounding particles may cause more collisions to occur. These examples indicate that there are many situations in which the particle–particle collisions play a significant role and show the importance of taking these collisions into account in a numerical simulation.

In the present paper, transient inhomogeneities in particle concentration distribution are examined. These inhomogeneities are induced by inter-particle collisions. Considering the pneumatic conveying of pulverized fuel to a burner, the consequence of such a time dependent in-homogeneous concentration distribution is that the burner will not constantly work at maximum efficiency. Furthermore, pressure fluctuations may arise that may cause vibrations or even damage. Hence it is important to understand, how inhomogeneities develop in time. The present work investigates the influence of particle loading on that effect for gas–solid flows in a horizontal channel.

Considering the Lagrangian type of simulation, i.e. the prediction of macroscopic properties of the dispersed phase by numerically solving the Lagrangian equation of motion of individual particles, various models have been proposed in order to account for inter-particle collisions. The distinct models are closely related to the way, the Lagrangian method is applied, which can be done in two principally different ways:

1. *Trajectory calculation (TC)*: A large number of individual particle trajectories is computed successively. Each trajectory represents a constant flow of particles with identical physical properties. The macroscopic properties of the particulate phase for a certain cell of the numerical mesh are computed by averaging over all trajectory segments that cross that cell. The application of the TC method is limited to the computation of steady flows.
2. *Simultaneous particle tracking (SPT)*: In the SPT method, the motion of a representative number of particles is calculated simultaneously. Each simulated particle represents a certain number of real particles with identical physical properties. This simulation method is inherently unsteady. The macroscopic properties of the particulate phase for a certain grid cell can be obtained at any time by averaging over all particles that are located in that cell at that point of time.

In order to take particle–particle collisions into account in the frame of the TC method Oesterlé and Petitjean (1991, 1993) presented an iterative simulation technique. In this technique, the collisions were treated stochastically on the basis of macroscopic particle properties obtained from the previous iteration. The technique was used to investigate a gas–solid flow in a horizontal pipe. The authors showed that collisions significantly influence the vertical concentration profile.

In the frame of the SPT method, collisions can be computed either deterministically or stochastically. Tanaka and Tsuji (1991) used a deterministic procedure to simulate a gas–solid flow in a vertical pipe. They found that for higher particle loading, the horizontal concentration distribution became more uniform compared to the dilute case. In their deterministic procedure, a collisionless time step was carried out initially for all particles. Thereafter for each pair of particles, it was examined whether these particles had collided

during the time step and, if yes, the collision was computed. The computational effort for this procedure is proportional to N^2, let N be the number of simulated particles. For this reason and with respect to the computer resources currently available, the deterministic calculation of collisions is of no practical relevance.

In majority of the applications of SPT method, collisions are treated stochastically. In that case, it takes advantage of the analogy between the motion of dispersed particles in gas–solid flows and the motion of molecules in dilute gas flows. For simulating the latter, the direct simulation Monte Carlo (DSMC) method was developed by Bird (1976, 1994). This simulation technique is based on the decoupling of molecular motion and collisions: In each time step, the collisionless motion of all the molecules is computed and after that a representative number of collisions is carried out by employing some kind of Monte Carlo method. The DSMC method has been applied to the simulation of gas-particle flows by several authors. Kitron et al. (1989,1990) investigated wall erosion, direct heat transfer and the concentration distribution of impinging streams, respectively. Tanaka et al. (1991) and Yonemura et al. (1993) examined gas-particle flows in vertical channels. They observed that the flow became unstable and inhomogeneous, as the gas velocity decreased with the increase in particle loading.

The present paper presents results of transient simulations of gas-particle flows in a horizontal channel. The particle motion was computed using the SPT simulation technique. Particle–particle collisions were accounted for by employing a stochastic model. Special emphasis was put on investigating the effect of particle loading on the formation and development of local regions of higher particle concentration, i.e. "clusters" of particles. A numerical simulation provides the advantage that certain physical effects can be "switched off" and thus effects can be studied seperately that cannot be segregated during an experiment. In reality, in flows with high loading inter-particle collisions as well as phase coupling play an important role. In the present work, only the effect of collisions on cluster formation was examined and the influence of phase coupling was not considered.

The basic equations of fluid motion and their numerical solution are briefly described in Section 2. In Section 3, the basic equations of particle motion are given. Furthermore, the application of the SPT technique and the stochastic collision model are described in detail. Finally in Section 4, results of test case calculations for the horizontal channel are presented and the effect of loading and collisions on the cluster formation is discussed.

2. Simulation of fluid motion

The basic equations describing the motion of an incompressible and isothermal gas are the continuity and the momentum equation. In the present work, the integral form of these equations is the starting point for their numerical solution. The integral form is obtained by formulating the mass and momentum balance for an infinitesimal control volume. For the present case the, continuity equation reads:

$$\int_S \rho_G \vec{v}_G \cdot \vec{n} \, dS = 0, \tag{1}$$

where ρ_G is the gas density, $\vec{v}_G$ is the gas velocity, S is the control volume's surface and $\vec{n}$ is the

normal vector belonging to the surface element dS. The integral form of the momentum equation reads:

$$\int_S \rho_G \vec{v}_G \vec{v}_G \cdot \ \vec{n}\, dS = \int_S \left(-p\bar{\bar{I}} + \bar{\bar{\tau}} \right) \cdot \vec{n}\, dS + \int_\Omega \rho_G \vec{g}\, d\Omega, \tag{2}$$

where p is the pressure, $\bar{\bar{I}}$ is the unit tensor, $\bar{\bar{\tau}}$ is the stress tensor, $\vec{g}$ is the gravitational acceleration and Ω is the control volume. As already mentioned, in the present work the motion of the gas phase is assumed to be steady and not affected by the presence of particles. Hence Eqs. (1) and (2) neither contain any time dependent terms nor any terms for considering mass or momentum transfer, respectively.

The above equations are solved numerically on the basis of Cartesian coordinates. Turbulence is accounted for by using a standard $k-\varepsilon$ model. The flow domain is discretized using block-structured, non-orthogonal, boundary-fitted grids. For discretizing the conservation equations, a finite-volume method is used along with a colocated variable arrangement. Pressure-velocity coupling is realized by employing a SIMPLE algorithm.

3. Simulation of the particulate phase

The motion of every single particle in the gas-particle flow is computed using the Lagrangian approach. The particles are assumed to be solid spheres and the density ratio of particle material and gas represented by $\rho_P/\rho_G \gg 1$. With that assumption, the Lagrangian equation of motion for a single particle of mass m_P reads:

$$m_P \frac{d\vec{v}_P}{dt} = \vec{F}_D + \vec{F}_M + \vec{F}_S + \vec{F}_{Gr}, \tag{3}$$

where $\vec{v}_P$ is the particle velocity, t is the time and the $\vec{F}_i$ denote the forces acting on the particle. The drag force $\vec{F}_D$ is calculated as:

$$\vec{F}_D = \frac{\pi}{8} \rho_G d_P^2 c_D v_{rel} \vec{v}_{rel}, \tag{4}$$

with d_P denotes the particle diameter, c_D the drag coefficient, $\vec{v}_{rel}$ the relative velocity between particle and gas and v_{rel} its absolute value. The drag coefficient c_D depends on the particle Reynolds number Re_P:

$$Re_P = \frac{d_P v_{rel}}{\nu_G}, \tag{5}$$

with ν_G denotes the kinematic viscosity of the gas. In the present work, the values for c_D proposed by Morsi and Alexander (1972) were used. The Magnus force $\vec{F}_M$ due to particle rotation is obtained from:

$$\vec{F}_M = \frac{\pi}{8} \rho_G d_P^2 c_M \frac{v_{rel}}{\omega_{rel}} \left(\vec{\omega}_{rel} \times \vec{v}_{rel} \right), \tag{6}$$

where $\vec{\omega}_{\mathrm{rel}}$ is the relative rotation between gas and particle:

$$\vec{\omega}_{\mathrm{rel}} = \vec{\omega}_{\mathrm{G}} - \vec{\omega}_{\mathrm{P}}, \quad \omega_{\mathrm{rel}} = |\vec{\omega}_{\mathrm{rel}}|, \tag{7}$$

with

$$\vec{\omega}_{\mathrm{G}} = \nabla \times \vec{v}_{\mathrm{G}} = \frac{\partial v_{\mathrm{G}}}{\partial x} - \frac{\partial u_{\mathrm{G}}}{\partial y}, \; \omega_{\mathrm{G}} = |\vec{\omega}_{\mathrm{G}}|, \tag{8}$$

and the coefficient c_{M} was chosen according to Tsuji et al. (1985). The Saffman force $\vec{F}_{\mathrm{S}}$ due to a shear gradient in the gas flow can be calculated from:

$$\vec{F}_{\mathrm{S}} = \frac{1}{4}\rho_{\mathrm{G}} d_{\mathrm{P}}^2 \sqrt{\nu_{\mathrm{G}}} \frac{1}{\sqrt{\omega_{\mathrm{G}}}} c_{\mathrm{S}} \left(\vec{v}_{\mathrm{rel}} \times \vec{\omega}_{\mathrm{G}}\right), \quad c_{\mathrm{S}} = 6.46. \tag{9}$$

This expression was derived under the assumption of $Re_{\mathrm{P}} \ll 1$, whereas Eq. (6) is valid for $Re_{\mathrm{P}} = 550$–1600. Therefore, these expressions are not consistent with each other. However, since the range of particle Reynolds number for the present test case was not known a priori, they were taken as an initial estimate of the transverse forces. This matter will be further discussed in Section 4.2.

The gravitational force $\vec{F}_{\mathrm{Gr}}$ is:

$$\vec{F}_{\mathrm{Gr}} = m_{\mathrm{P}} \vec{g} = \frac{\pi}{6} \rho_{\mathrm{P}} d_{\mathrm{P}}^3 \vec{g}. \tag{10}$$

Other forces like added-mass force or Basset force can be neglected under the assumption of $\rho_{\mathrm{P}}/\rho_{\mathrm{G}} \gg 1$.

In order to compute $\vec{F}_{\mathrm{M}}$ the particle's rotational velocity $\vec{\omega}_{\mathrm{P}}$ must be known. $\vec{\omega}_{\mathrm{P}}$ can be calculated from:

$$I_{\mathrm{P}} \frac{\mathrm{d}\vec{\omega}_{\mathrm{P}}}{\mathrm{d}t} = \frac{\rho_{\mathrm{G}}}{2} \left(\frac{d_{\mathrm{P}}}{2}\right)^5 c_{\omega} \omega_{\mathrm{rel}} \vec{\omega}_{\mathrm{rel}}, \tag{11}$$

where $I_{\mathrm{P}} = 1/10 m_{\mathrm{P}} d_{\mathrm{P}}^2$ is the particle's moment of inertia and the right hand side of Eq. (11) denotes the torque exerted on the particle by the fluid as proposed by Dennis et al. (1980).

The turbulent velocity fluctuations of the gas phase were accounted for by using the Lagrangian Stochastic-deterministic (LSD) model by Milojevic (1990). The integral time scale of fluid turbulence is obtained from:

$$T_{\mathrm{E}} = c_{\mathrm{E}} \frac{k}{\varepsilon}, \qquad c_{\mathrm{E}} = 0.3, \tag{12}$$

and the integral length scale is:

$$L_{\mathrm{E}} = T_{\mathrm{E}} \sqrt{\frac{2}{3} k}. \tag{13}$$

The mean time, a particle takes to cross a turbulent eddy can be estimated by:

$$T_{\mathrm{Cr}} = \frac{L_{\mathrm{E}}}{v_{\mathrm{rel}}}, \tag{14}$$

and the mean interaction time T_i of a particle with a turbulent eddy is:

$$T_i = \min(T_{\mathrm{E}}, T_{\mathrm{Cr}}). \tag{15}$$

In order to simulate the wall roughness, a model employing an inclined virtual wall as proposed by Sommerfeld (1992) was used. The wall model parameters used here are given in Table 1.

3.1. The motion of the particle phase

3.1.1. Simulation principle

As already mentioned, the formation of particle clusters in gas-particle channel flow was investigated. Such kind of cluster formation was observed by Yonemura et al. (1993), who examined upward flows in vertical channels. In their simulation experiments, they inserted particles at the bottom of the channels, maintaining a constant mass flow. They found that in the upper part of the channels, the flow became in-homogeneous and unstable in space and time, as the gas velocity decreased and the particle loading increased. Furthermore, Yonemura

Table 1
Physical and numerical simulation parameters

Property	Symbol	Value
Channel height	h	0.03 m
Channel length	l	0.8 m
Gas density	ρ_{G}	1.21 kg/m^3
Kinematic viscosity of gas	ν_{G}	1.48×10^{-5} m^2/s
Gas bulk velocity	U_{G}	25.5 m/s
Mean particle diameter	$\bar{d}_{\mathrm{P}}$	100 μm
Particle material density	ρ_{P}	2620 kg/m^3
Particle relaxation time	τ_R	0.08 s
Particle terminal velocity	v_t	1 m/s
Coefficient of restitution for particle-wall collision	e_W	0.9
Coefficient of friction for particle-wall collision	f_W	0.53
Mean inclination angle of virtual wall	γ	0°
Roughness height of channel wall	H_r	30 μm
Standard deviation of roughness height	ΔH_r	5.3 μm
Roughness length of channel wall	L_r	300 μm
Coefficient of restitution for particle–particle collision	e_{P}	0.95
Coefficient of friction for particle–particle collision	f_{P}	0.4
Mass loading ratio	η	0.01, 1, 2, 5, 10
Number of grid cells	–	128×16
Total number of simulated particles	$N_{\mathrm{P,\,tot}}$	10000
Time step	Δt	2×10^{-5} s

et al. (1993) showed that the coefficients of restitution e_P and friction f_P for the inter-particle collisions largely affect the growth of clusters.

In contrast to the work of Yonemura et al. (1993), only the effect of particle–particle collisions was examined here and the change of gas velocity due to the presence of particles was not accounted for. In reality, there is always a strong phase coupling, if, the particle concentration is as high as in the flows considered here. However, the aim of the present work is to contribute to a better understanding of the mechanisms leading to cluster formation. Therefore, the advantage is that in a numerical simulation, certain physical effects can be examined separately.

The formation and development of particle clusters in both space and time is a transient process. For this reason, the motion of particles must be calculated as a function of time, even if the gas flow is assumed to be steady. The transient particle motion can be computed by applying the SPT simulation technique, i.e. the simultaneous computation of the motion of all the simulated particles. The application of the SPT technique along with a stochastic treatment of particle–particle collisions is often referred to as the DSMC method. This method was first proposed by Bird (1976, 1994) for the simulation of dilute gas flows. In the present work, the following technique was used:

1. A representative number of particles is considered in the simulation, i.e. each simulated particle represents a certain number of real particles.
2. The transient motion of the particle phase is simulated by computing the motion of all particles in successive time steps.
3. The motion of each particle during a single time step Δt is assumed to be decoupled from inter-particle collisions. This assumption is valid if, Δt is small compared to mean time between collisions. If a particle collides with a channel wall during Δt, the particle-wall collision is carried out according to the rough-wall model mentioned above. Following which, the calculation of particle motion is continued for the remaining part of the time step.
4. After computing the collisionless motion of a single particle during Δt, a stochastic procedure is applied to that particle to account for collisions. This procedure is described in the next subsection.

The flow domain is divided into cells, which are small as compared to the spatial changes in the gas flow. The local macroscopic properties of the dispersed phase at a certain time are obtained by averaging over all particles, that are located in the same cell at that time.

3.1.2. Treatment of collisions

If motion of all the particles is calculated simultaneously, it is theoretically possible to treat the collisions deterministically. Therefore, after every time step one has to examine for every pair of particles in the flow field to check for any contact point during the previous step. If such a point is found, the collision between the two particles can be easily computed. This kind of deterministic procedure was used by Tanaka and Tsuji (1991) for simulating gas-particle flows in a vertical pipe. However, this way of treating collisions causes a numerical effort, which is proportional to the square of the total number of particles. Even if only the paths of near neighbours, say of all the particles in one cell, are compared, there is still a

proportionality to the total number of molecules in the cell. In order to reduce the numerical effort to a linear proportionality, several stochastic procedures have been proposed. In the frame of the DSMC method, the time-counter method and the no-time-counter method were developed by Bird (1976, 1989). The time-counter method was also applied to the simulation of gas–solid flows by Kitron et al. (1989, 1990). Yonemura et al. (1993) used in their simulations the modified Nanbu method proposed by Illner and Neunzert (1987). All these methods are based on randomly selecting a pair of particles that are located in the same cell, computing a collision probability for that selected pair and carrying out the collision according to the acceptance–rejection method. The methods differ in the way of determining how many collisions are actually carried out.

In the present work, a stochastic model was used with collisions taking place not between two actually simulated particles but between one simulated and one virtual particle. As decribed above for each time step Δt, the motion of all particles in that time step was calculated successively. In order to account for the collisions for every particle, a stochastic procedure was applied after calculating the collisionless motion of that particle. Considering the two-dimensional case shown in Fig. 1, the effective area A_{eff} swept out by the particle in the time step Δt, which is small as compared to the mean time between collisions τ_c, is:

$$A_{\text{eff}} = d_{\text{eff}} v_r \Delta t, \tag{16}$$

where d_{eff} is the effective diameter:

$$d_{\text{eff}} = d_{\text{P}} + d_{P0}, \tag{17}$$

with d_{P0} denoting the mean particle diameter in the surrounding particle cloud, and v_r is the absolute value of the relative velocity between the particle and the surrounding particle cloud:

$$v_r = |\vec{v}_r| = |\vec{v}_{\text{P}} - \vec{v}_{P0}|, \tag{18}$$

with $\vec{v}_{P0}$ denoting the mean velocity of particles in the cloud. The "surrounding cloud" is

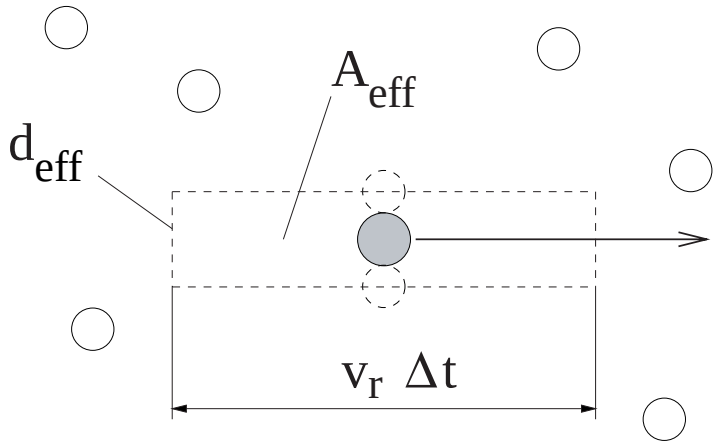

Fig. 1. Effective area swept out by a particle moving in a surrounding particle cloud.

assumed to consist of all particles in the cell and the particle is located at the end of the time step. Hence, d_{P0} and $\vec{v}_{P0}$ are obtained by averaging over all particles in the current cell. The number of particles $N_{A_{\text{eff}}}$ that are located in the area A_{eff} and thus the number of collisions with other particles in Δt can be computed from the local number density n_{P0}:

$$N_{A_{\text{eff}}} = n_{P0} A_{\text{eff}}. \tag{19}$$

Dividing this value by Δt results in the local collision frequency ν_c, i.e. the number of collisions per unit time:

$$\nu_c = n_{\text{P0}}(d_{\text{P}} + d_{\text{P0}})|\vec{v}_{\text{P}} - \vec{v}_{\text{P0}}|. \tag{20}$$

After computing the collision frequency, the collision probability P_c, i.e the probability that the particle undergoes a collision in Δt, is computed as proposed by Oesterlé and Petitjean (1993):

$$P_c = 1 - \mathrm{e}^{-\nu_c \Delta t}. \tag{21}$$

The acceptance-rejection method is used to decide, whether a collision actually takes place or not. Therefore, a random number $\Psi \in [0,1]$ is generated from a uniform distribution. A collision is decided to take place if $P_c > \Psi$.

As already mentioned above, the collision is carried out between the particle currently under consideration and a virtual collision partner. The physical properties of the virtual partner like diameter, velocity and angular velocity are chosen according to the mean values for the current cell. The collision configuration as shown in Fig. 2 is chosen randomly by generating a collision angle $\varphi \in [-\pi/2,\pi/2]$ from a uniform distribution. The particle's location remains

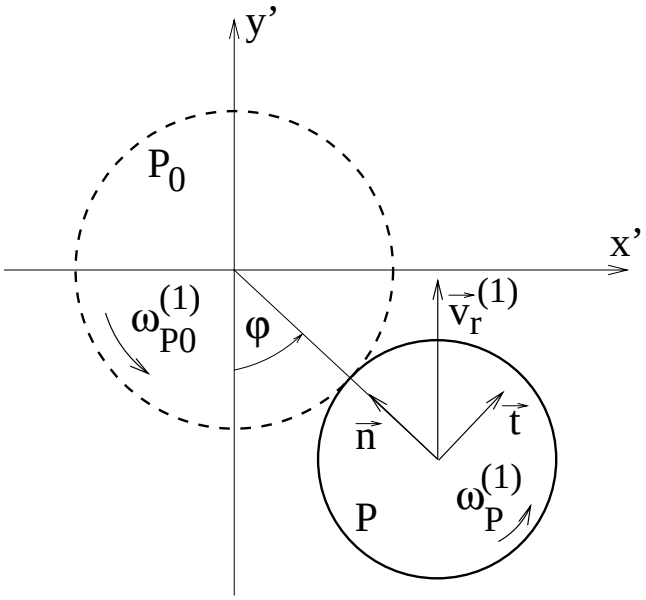

Fig. 2. Collision configuration for particle P colliding with virtual particle P0.

unchanged during the collision and the post-collision velocity and angular velocity are computed. Since the particle density ρ_P is much larger than the gas density ρ_G, the collision time is much shorter than the particle relaxation time. Hence, fluid forces can be neglected during the collision. The post-collision velocities and angular velocities can be calculated by applying the equations of momentum and angular momentum, respectively:

$$\vec{v}_P^{(2)} = \vec{v}_P^{(1)} + \frac{1}{m_P}\vec{J}, \tag{22}$$

$$\vec{v}_{P0}^{(2)} = \vec{v}_{P0}^{(1)} - \frac{1}{m_{P0}}\vec{J}, \tag{23}$$

$$\vec{\omega}_P^{(2)} = \vec{\omega}_P^{(1)} + \frac{d_P}{2I_P}(\vec{n} \times \vec{J}), \tag{24}$$

$$\vec{\omega}_{P0}^{(2)} = \vec{\omega}_{P0}^{(1)} + \frac{d_{P0}}{2I_{P0}}(\vec{n} \times \vec{J}). \tag{25}$$

Here the subscript 'P' denotes the particle under consideration, the subscript 'P0' denotes the virtual particle, the superscripts (1) and (2) denote variable values before and after the collision, respectively, $\vec{n}$ is the normal vector of unit length directed from the centre of particle P to the centre of particle P0 (see Fig. 2) and $\vec{J}$ is the impulsive force exerted on particle P during the collision. $\vec{J}$ can be decomposed into its normal and tangential components:

$$\vec{J} = J_n\vec{n} + J_t\vec{t}, \tag{26}$$

where $\vec{t}$ is the tangential unit vector pointing in the same direction as the tangential component of the relative velocity between the particles $\vec{v}_r^{(1)}$. By subtracting Eq. (23) from Eq. (22), multiplying the resulting equation with $\vec{n}$ and using the relation between the normal components of the pre- and post-collision relative velocities:

$$\vec{v}_r^{(2)} \cdot \vec{n} = -e_P\left(\vec{v}_r^{(1)} \cdot \vec{n}\right), \tag{27}$$

with e_P denoting the coefficient of restitution, the normal component of $\vec{J}$ is obtained by:

$$J_n = -\frac{(1+e_P)\left(\vec{v}_r^{(1)} \cdot \vec{n}\right)}{\frac{1}{m_P} + \frac{1}{m_{P0}}}. \tag{28}$$

Note that J_n is always negative, since $(\vec{v}_r^{(1)} \cdot \vec{n})$ is always positive by definition, i.e. the normal component of $\vec{J}$ is always directed towards the centre of particle P. The slip velocity, i.e. the relative velocity between the surfaces of P and P0, is given by:

$$v_{\mathrm{sl}} = \begin{cases} \vec{v}_r^{(1)} \cdot \vec{t} - \omega_{\mathrm{P}} \dfrac{d_{\mathrm{P}}}{2} - \omega_{\mathrm{P0}} \dfrac{d_{\mathrm{P0}}}{2} & \text{for } \varphi \geq 0, \\ \vec{v}_r^{(1)} \cdot \vec{t} + \omega_{\mathrm{P}} \dfrac{d_{\mathrm{P}}}{2} + \omega_{\mathrm{P0}} \dfrac{d_{\mathrm{P0}}}{2} & \text{for } \varphi < 0. \end{cases} \tag{29}$$

v_{sl} is defined as being positive if it is directed along the same direction as the tangential vector $\vec{t}$. Note that $(\vec{v}_r^{(1)} \cdot \vec{t})$ is always positive by definition (see Fig. 2). In order to calculate the tangential component of $\vec{J}$, it must be distinguished between non-sliding and sliding collision, i.e. whether the initial slip between the particle surfaces ceases or not. As shown by Tanaka and Tsuji (1991) and Oesterlé and Petitjean (1993) these cases can be determined by:

1. Sliding collision for $0 < |J_n| \leq \dfrac{2|v_{\mathrm{sl}}|}{7f_{\mathrm{P}}\left(\frac{1}{m_{\mathrm{P}}}+\frac{1}{m_{\mathrm{P0}}}\right)}$: $\quad |J_t| = f_P |J_n|,$ (30)

2. Non-sliding collision for $|J_n| > \dfrac{2|v_{\mathrm{sl}}|}{7f_{\mathrm{P}}\left(\frac{1}{m_{\mathrm{P}}}+\frac{1}{m_{\mathrm{P0}}}\right)}$: $\quad |J_t| = \dfrac{2|v_{\mathrm{sl}}|}{7\left(\frac{1}{m_{\mathrm{P}}}+\frac{1}{m_{\mathrm{P0}}}\right)},$ (31)

where f_{P} denotes the coefficient of friction. J_t is always directed opposite to the direction of slip velocity and is given by:

$$J_t = \begin{cases} -|J_t| & \text{for } v_{\mathrm{sl}} \geq 0, \\ |J_t| & \text{for } v_{\mathrm{sl}} < 0, \end{cases} \tag{32}$$

where a positive value of J_t indicates that it points in the same direction as $\vec{t}$. Thus the impulsive force $\vec{J}$ is completely given and by replacing it in Eqs. (22) and (24), the post-collision velocity and angular velocity of the particle P can be computed.

4. Results

4.1. Description of test case

Test case calculations were carried out for gas-particle flows in a horizontal channel. A sketch of the channel geometry is given in Fig. 3. As shown in this figure, the flow is simulated

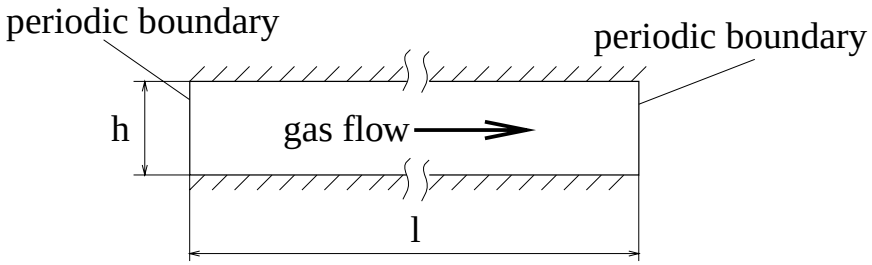

Fig. 3. Geometry of horizontal channel for simulation.

only in a segment of the channel and periodic boundary conditions are used at the left and right boundary of the geometry. Any particle that crosses one of these boundaries is inserted again at the opposite boundary by retaining all of its current physical properties.

The gas velocity and turbulence properties were assumed to be identical to a developed turbulent channel flow and constant over the channel length. These properties were obtained in a preliminary calculation. As mentioned above, despite the relatively high particle loading considered in this work, the gas flow properties remained unchanged in the simulations to investigate just the effect of inter-particle collisions.

The physical and numerical parameters used in the present simulations are summarized in Table 1. Most of the physical parameters were chosen according to Oesterlé and Petitjean (1993), who carried out simulations for horizontal pipe flows. The particle size distribution was assumed to be Gaussian with a mean diameter of $\overline{d}_P = 100$ μm and a standard deviation of $\Delta d_P = 20$ μm. In the present work, flows with different mass loading ratios η were computed. For $\eta = 0.01$, the flow was assumed to be dilute and particle–particle collisions were not considered. For all other loading ratios, collisions were simulated according to the stochastic procedure described above. The particles' initial locations were distributed randomly across the flow domain to achieve a uniform initial concentration distribution. The initial axial velocity was chosen as 0 m/s and the transverse velocity was obtained as a random number from a Gaussian distribution with a mean value of 0 m/s and a standard deviation of 1 m/s.

The use of periodic boundary conditions implies that the total number of simulated particles in the flow domain, $N_{P,\,tot}$, remains constant throughout the computation. Also the mean particle number density, n_{P0}, i.e. the mean number of particles per unit volume, remains constant, whereas the local number density, n_P, changes. The particles are re-distributed in the course of a simulation due to fluid forces, gravity, particle–wall collisions and particle–particle collisions.

4.2. Results of simulations

In Fig. 4, the vertical distribution of the relative number density n_P/n_{P0} is shown for different mass loading ratios. The results obtained are compared to those obtained by Oesterlé and Petitjean (1993) for a horizontal pipe flow by applying the trajectory calculation technique. The data of Oesterlé and Petitjean (1993) was taken at a distance of $L = 6$ m from the inlet cross section of the pipe. In preliminary simulations, it had been found that the average time particles need to move that distance under the given conditions is $t = 0.3$ s. Accordingly, this period of time was chosen as the total physical time to elapse in one simulation run. The two-dimensional distribution of relative number density at $t = 0.3$ s was averaged in axial direction for different distances from the channel bottom and the resulting vertical concentration distribution is shown in Fig. 4.

For the dilute case $\eta = 0.01$, the particle concentration is almost uniformly distributed over channel height. The particles in the flow are strongly re-suspended due to collisions with the rough walls at the channel top and bottom. For the pipe flow, the number density in the lower part of the pipe is higher than in the upper part. In contrast to the two-dimensional simulations of the present work, in a three-dimensional pipe, a particle colliding with a wall has one more degrees of freedom concerning the post-collision translational velocity. For this

reason, the vertical component of the post-collision velocity is generally smaller in a pipe, than what it is in a channel. Hence re-bounding particles in a pipe flow reach only a smaller height and the particle concentration in the lower region is higher.

With an increasing particle loading, the concentration profile becomes more non-uniform. The concentration in the upper part decreases with an increase in the lower part. This effect is caused by particle–particle collisions. Particles moving upwards after bouncing against the bottom wall collide with other particles in the inner region of the flow field. As a consequence, the maximum height these rebounding particles are able to reach is smaller than in the collisionless case and thus particles tend to concentrate in the lower part of the flow domain. Under certain conditions, the maximum number density is observed not closest to the channel bottom but at a certain distance from that wall (see results for channel flow for $\eta = 5, \eta = 10$, and for pipe flow for $\eta = 2, \eta = 10$). In these cases, a kind of "shielding" effect occurs. Rebounding particles that move upwards meet particles moving downwards due to gravity. A zone develops, where a large number of inter-particle collisions take place. Due to these collisions, the vertical velocity component of upward moving particles is reduced and likewise

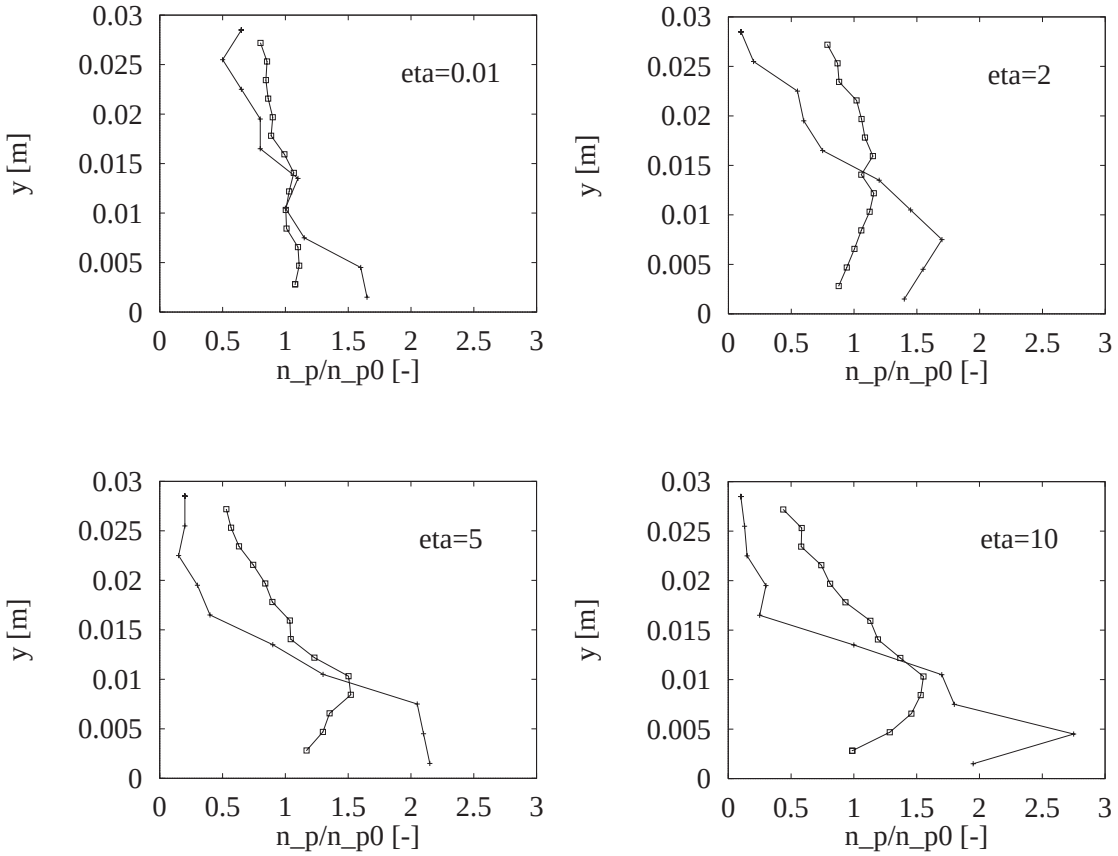

Fig. 4. Vertical distribution of relative number density; this work ($t = 0.3$ s) and trajectory calculation by Osterle and Petitjean (1993) for horizontal pipe ($L = 6$ m).

the vertical velocity component of downward moving particles. As a consequence, a region of higher particle concentration develops and the bottom wall is protected from the impacting particles. A similar kind of shielding effect was reported by Kitron et al. (1989).

In Fig. 5, the profile of the mean axial velocity is shown for different loading ratios and for comparison also, the gas velocity profile is shown. Like the concentration profile discussed above also the velocity profile was obtained at $t = 0.3$ s by averaging the local velocity in axial direction. In the dilute case, the maximum axial velocity is observed below the channel axis, whereas in all other cases, the maximum velocity is found closer to the axis. In all the cases, the velocity decreases towards the channel walls. This is due to the particle-wall collisions, which because of friction and in-elasticity reduce the particles' kinetic energy. Hence, after a wall collision occurs, a particle's absolute velocity is lower than before and the particle is accelerated again by the gas flow, as it moves back from the wall into the flow field. In Fig. 5, it can also be seen that the particles' mean axial velocity increases, as the loading increases. With an increasing loading, the particles undergo more and more inter-particle collisions. These collisions cause the vertical component of particle motion to be damped. As a result, the number of collisions with the channel walls decreases. In other words, the mean time between two wall collisions increases. Hence the particles spend more time in the inner region of the flow field and can be accelerated by the gas up to a higher velocity.

The particle velocity fluctuations in axial direction, $\sqrt{\overline{u_{\mathrm{P}}'2}}$, and in vertical direction, $\sqrt{\overline{v_{\mathrm{P}}'2}}$, are shown in Fig. 6. Both these components are found to be reduced, as the particle loading increases. For the present test case, the deviation of a particle's velocity from the mean flow velocity is mainly caused by the particle's collisions with the channel walls. As the particle loading increases, a particle collides more often with other particles. These collisions reduce the

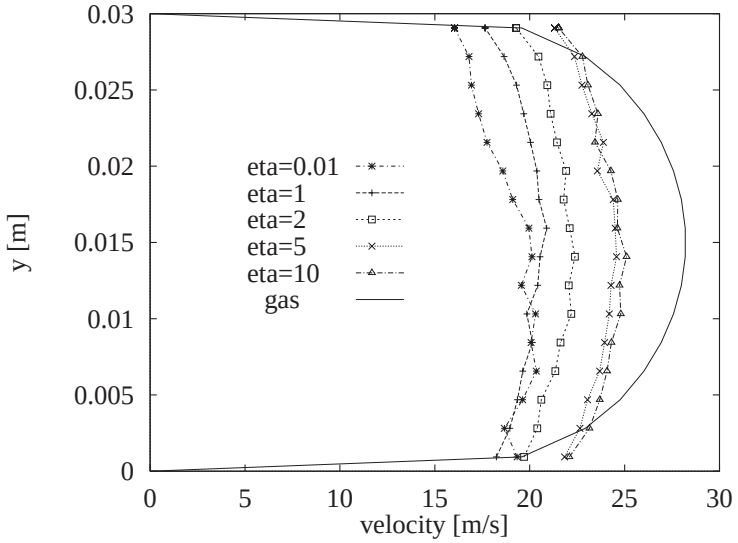

Fig. 5. Vertical distribution of mean axial velocity.

particle's vertical velocity component, resulting in less frequent wall collisions, and thus a reduction of velocity fluctuations.

For the dilute case, $\eta = 0.01$, $\sqrt{\overline{u_P'^2}}$ is about twice as large as $\sqrt{\overline{v_P'^2}}$. The difference between the two fluctuation components becomes smaller with increasing loading. For $\eta = 10$, both the components are almost equal. This is consistent with the results of Tanaka and Tsuji (1991) for a vertical pipe flow. Due to inter-particle collisions, which occur more frequently at higher loadings, particle momentum is increasingly exchanged and redistributed among the particles, as the loading increases.

The range of the particle Reynolds number for the present simulations was found to be $Re_P \approx 10$–200. Hence Eqs. (6) and (9), which were taken as estimates for the lift forces, are not applicable. However, as an effect of gravity and irregular bouncing with the channel walls, the motion of the particles is a zig-zag motion. That is, while moving in the direction of the mean

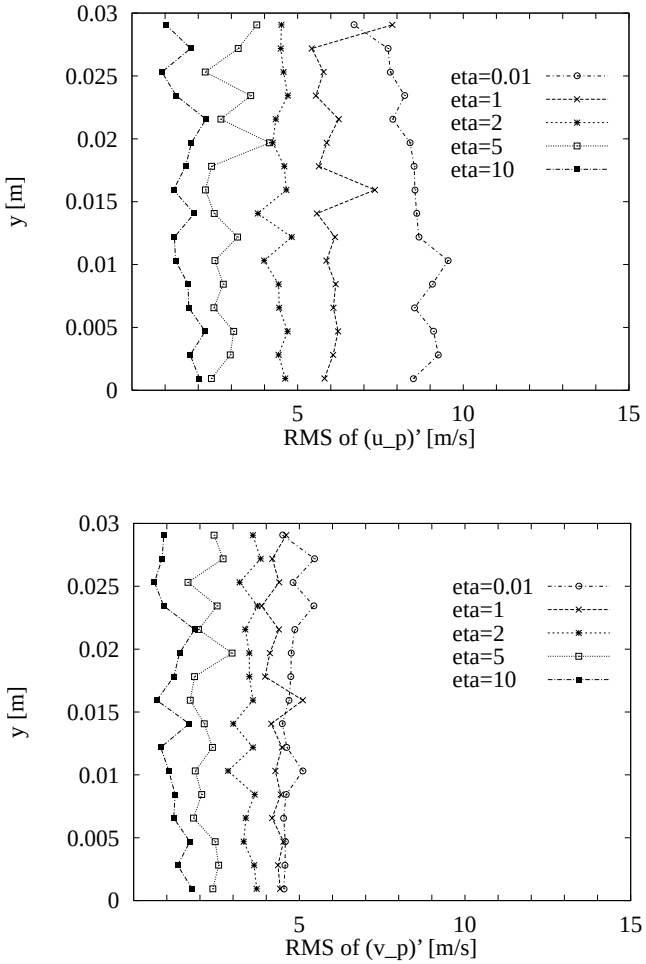

Fig. 6. Vertical distribution of particle velocity fluctuation; top: axial component $\sqrt{\overline{u_P'^2}}$; bottom: vertical component $\sqrt{\overline{v_P'^2}}$.

flow, particles undergo frequent collisions alternately with the bottom and top channel walls. For the dilute case, the mean absolute value of the particle vertical velocity component is $|\overline{v_P}| = 2.2$ m/s. The average time gap between two wall collisions is 0.01 s, which is well below the particle relaxation time. As the particle loading increases, the average time between wall collisions increases as well. At the same time, the mean time between particle–particle collisions decreases. For a mass loading ratio of $\eta = 10$, the mean time between inter-particle collisions is of the order of 10^{-3}–10^{-2} s, which again is well below the particle relaxation time. Hence it can be assumed that for any case, the inertial effects and/or the effects of particle–particle collisions are dominant and the effects of the aerodynamic lift forces can be neglected. For this reason, the error made by the wrong estimate of the lift forces is believed to have no impact on the computed results.

The integral time scale T_E of fluid turbulence for the present channel flow is of the order of 10^{-3} s, and the integral length scale L_E is of the order of 10^{-3} m. Considering the mean absolute value of the particle vertical velocity component of $|\overline{v_P}| = 2.2$ m/s, the mean crossing time T_{Cr} is also found to be of the order of 10^{-3}s. Both T_E and T_{Cr} are more than an order of magnitude smaller than the particle relaxation time, which in the present case is $\tau_R = 0.08$ s.

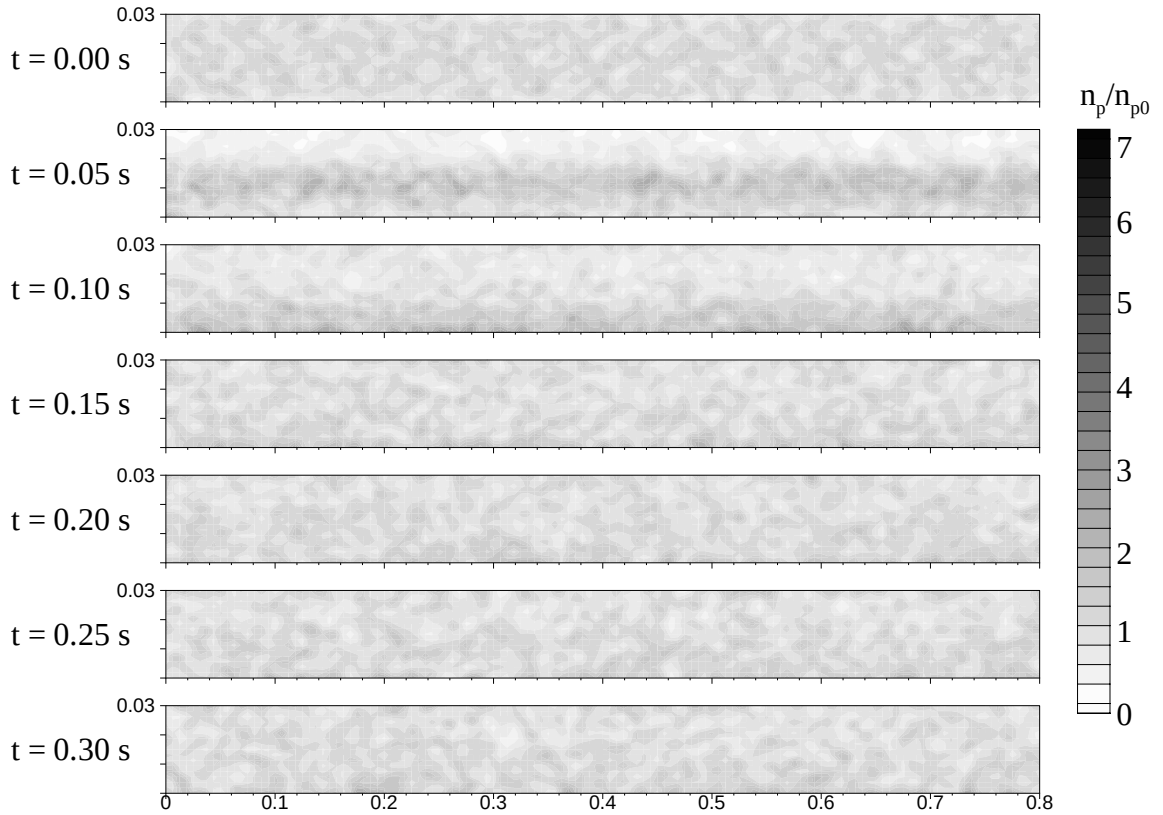

Fig. 7. Distribution of relative number density over time for $\eta = 0.01$.

Therefore, it can be assumed that the turbulent fluctuations of the gas velocity only have a minor influence on the particle motion.

The development of particle concentration distribution in space and time for the different loading ratios is shown in Figs. 7–11. In each of these figures the distribution of relative number density n_P/n_{P0} in the channel is given at seven different times. Note that for the reason of a more convenient representation, the channel geometry is shown compressed in horizontal direction. As mentioned above, all simulations start with a randomly generated particle distribution, i.e. at $t = 0$ s is $n_P/n_{P0} \approx 1$ all across the channel. After starting the simulation, the particles are accelerated in a horizontal direction by fluid forces and in downward direction by gravity. The latter is the reason for the increase of number density in the lower half of the channel, which can be observed for all loading ratios at $t = 0.05$ s. For the dilute case $\eta = 0.01$, which is shown in Fig. 7, this in-homogeneity in the vertical concentration distribution can still be found at $t = 0.1$ s. As the simulation for $\eta = 0.01$ progresses further, the concentration becomes almost uniform again, because the particles are redispersed due to irregular bouncing with the channel walls.

In contrast to the dilute case for the cases of $\eta = 1$ and $\eta = 2$ the inhomogeneity in vertical

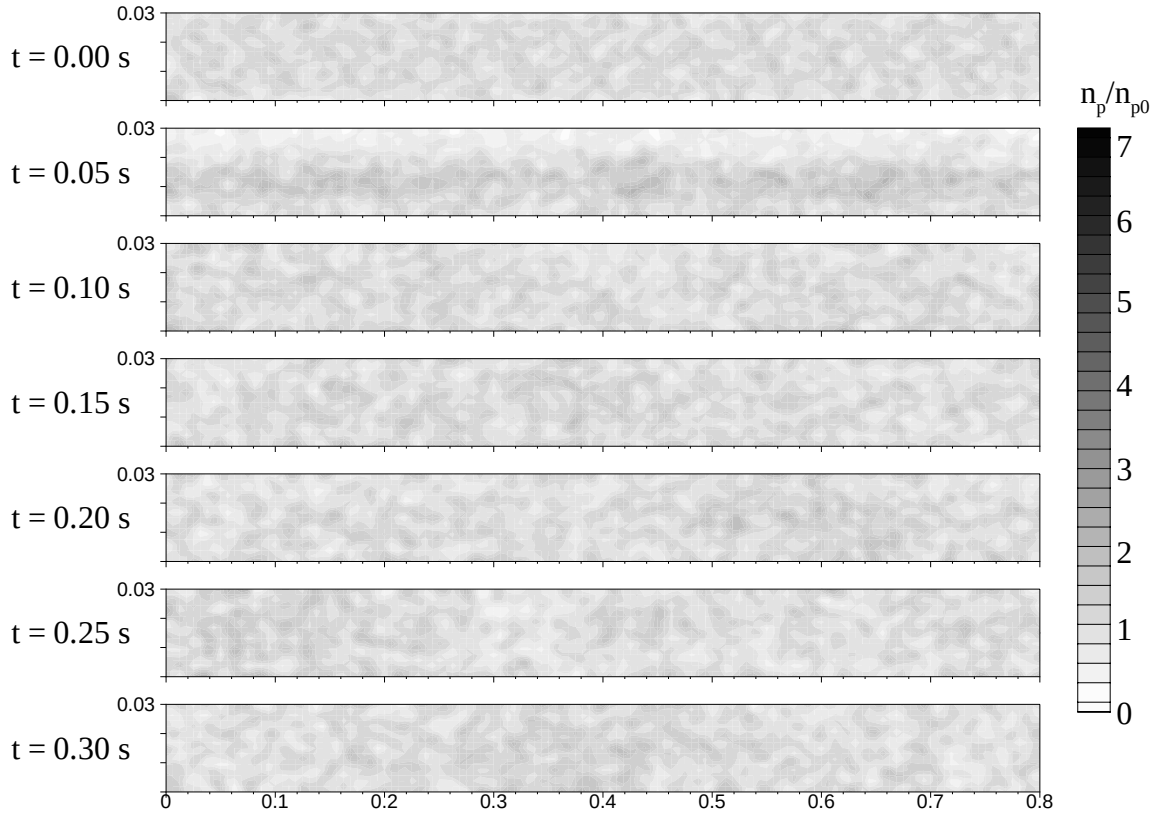

Fig. 8. Distribution of relative number density over time for $\eta = 1$.

concentration distribution is not observed anymore at $t = 0.1$ s (see Figs. 8 and 9, respectively). Obviously, for these loading ratios particles are redispersed quicker. This is a result of the momentum exchange induced by particle–particle collisions. Particles that have bounced against the bottom wall in an early stage of the simulation move upwards and collide with particles that still move downwards. Thus particles are redistributed evenly. For $\eta = 1$, the concentration distribution remains almost uniform throughout the rest of the simulation. For $\eta = 2$, the development of a region of higher concentration can be observed. The center of this region is located close to the channel axis and the maximum number density in this region is about three times higher than the mean number density.

For the loading ratios of $\eta = 5$ (see Fig. 10) and $\eta = 10$ (see Fig. 11), the inhomogeneity of concentration distribution in vertical direction at $t = 0.05$ s appears more distinct than in the cases discussed before. Furthermore, the inhomogeneity does not vanish in the course of the simulation. The particle flow becomes even more and more inhomogeneous also in horizontal direction. Local areas of high concentration develop; where the relative number density rises up to $n_P/n_{P0} \approx 7$. These areas may be called "clusters", although in a non-compressed image, they rather look like "garlands". Clusters seem to formate and grow around "cores", i.e. small local areas of higher number density induced by stochastic concentration fluctuations. Particles

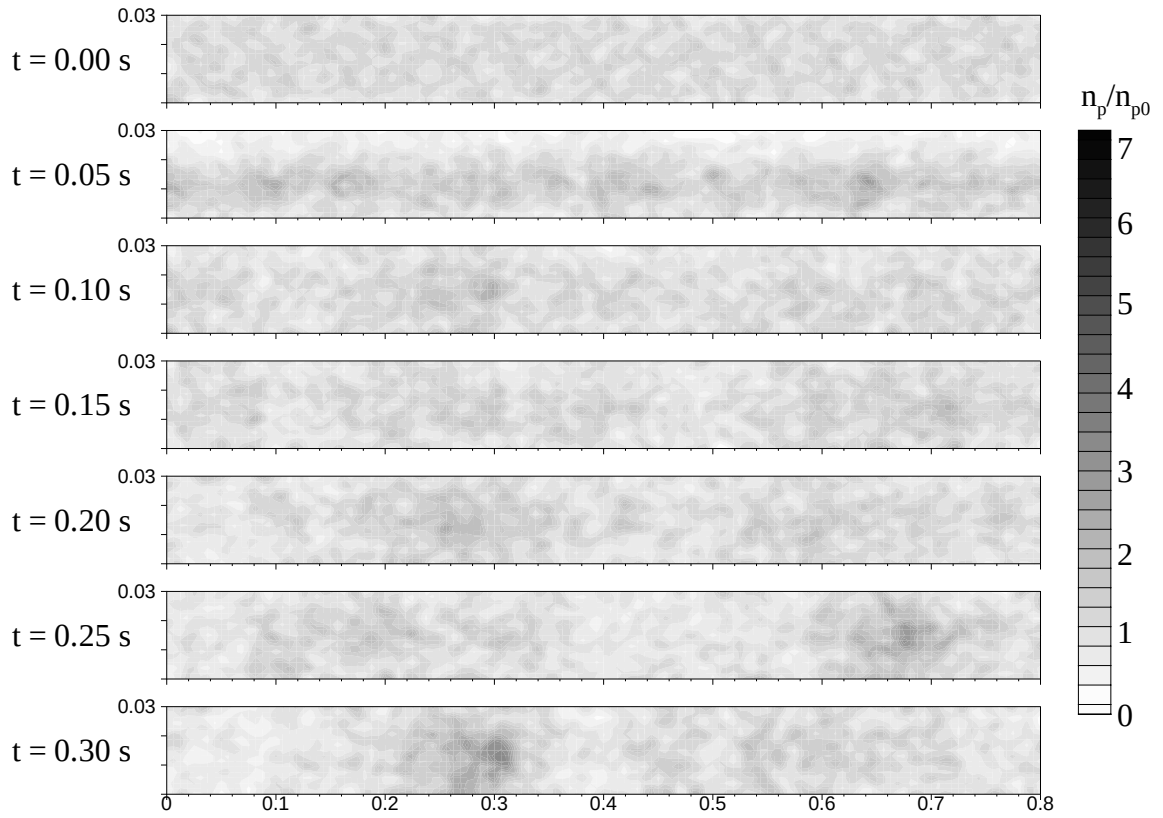

Fig. 9. Distribution of relative number density over time for $\eta = 2$.

penetrating a cluster can be "captured", since the large number of collisions they undergo there cause their momentum to be adapted to that of the cluster particles. The center of most clusters is located between the channel axis and the bottom wall. This corresponds to the horizontally averaged data shown in Fig. 4. As one can see in Figs. 10 and 11, clusters do not constantly grow, but also thin and vanish. In the process of cluster breakup, the interaction of cluster particles with the bottom wall seems to play an important role.

A quantitative measure of the inhomogeneity of concentration distribution is given by the root mean square of the fluctuation of relative number density $n_{fluct,\,RMS}$, which is computed as follows:

$$n_{\text{fluct, RMS}} = \sqrt{\overline{\left(\frac{n_{\text{P}}}{n_{\text{P0}}} - 1\right)^2}}. \tag{33}$$

In Fig. 12 $n_{\text{fluct, RMS}}$ is shown, as it develops in time for all loading ratios considered in this paper. The value of $n_{\text{fluct, RMS}}$ at $t = 0$ s corresponds to the homogeneous concentration distribution obtained by randomly distributing the particles in the flow field. As already seen in Figs. 7–11, inhomogeneity increases at the beginning of the simulation for all loading ratios.

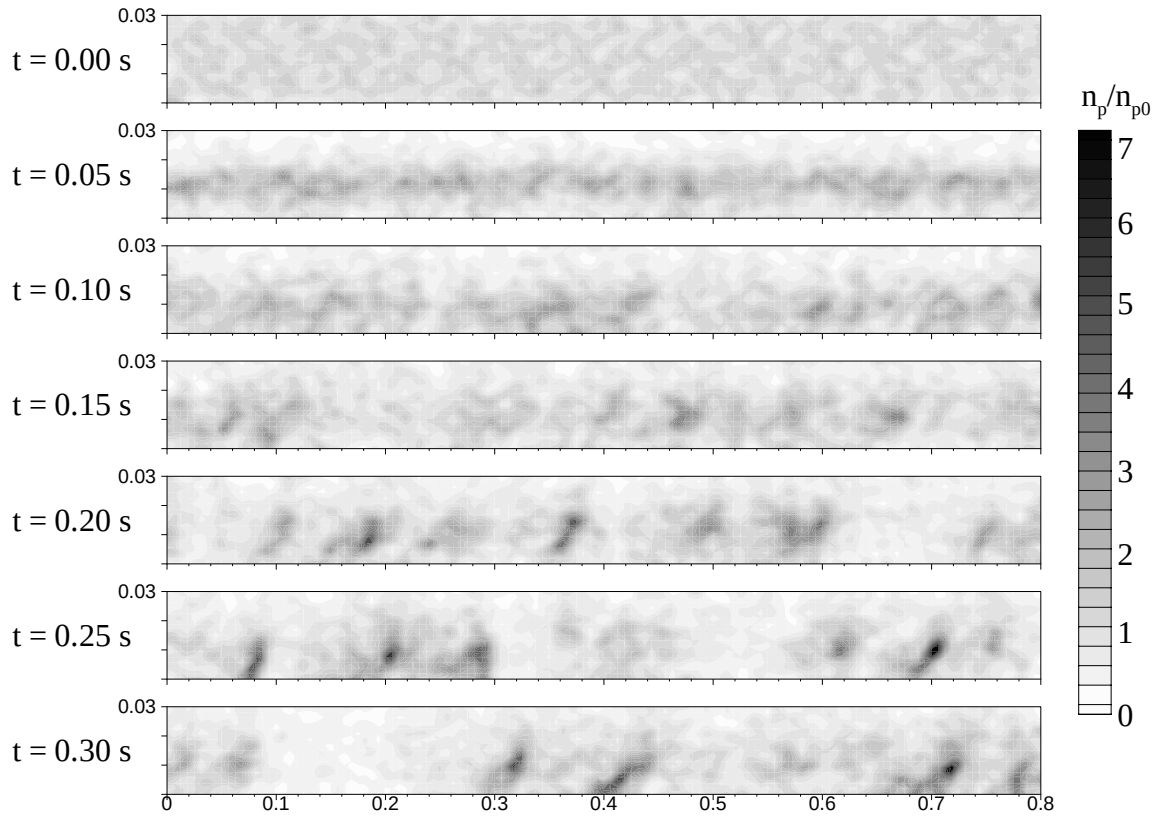

Fig. 10. Distribution of relative number density over time for $\eta = 5$.

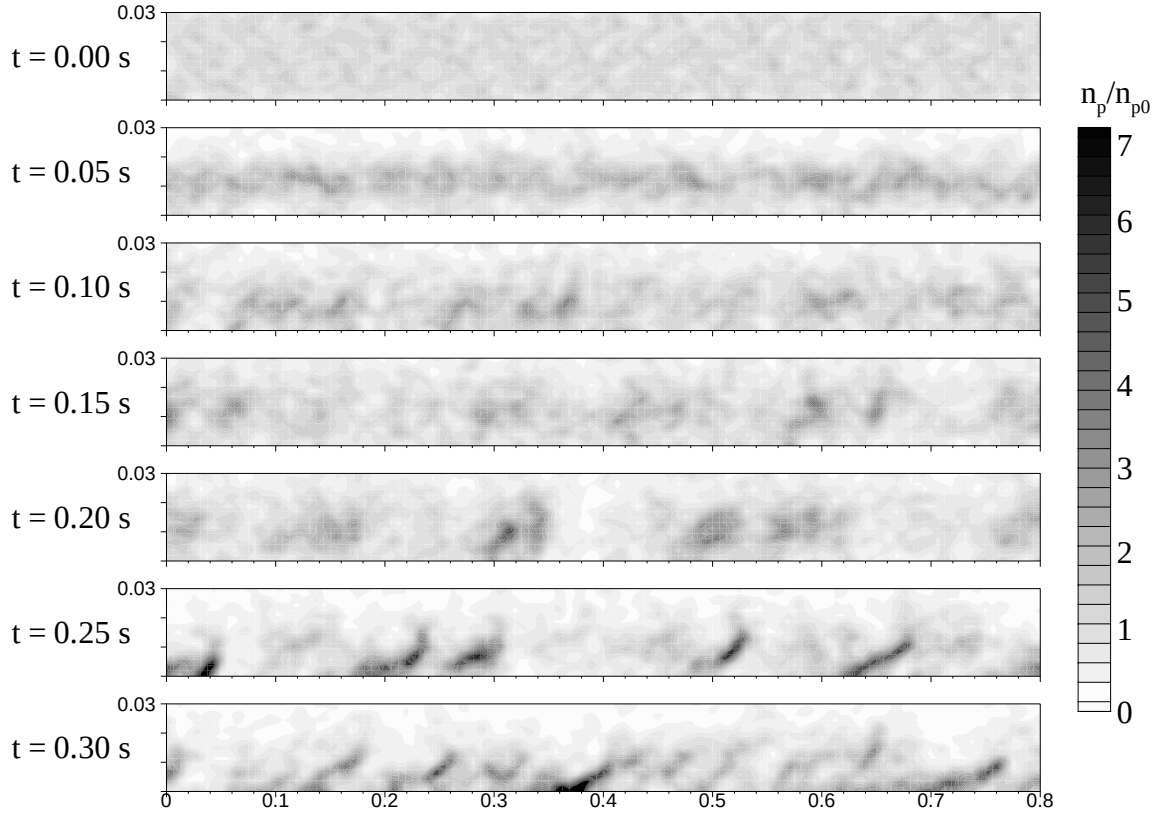

Fig. 11. Distribution of relative number density over time for $\eta = 10$.

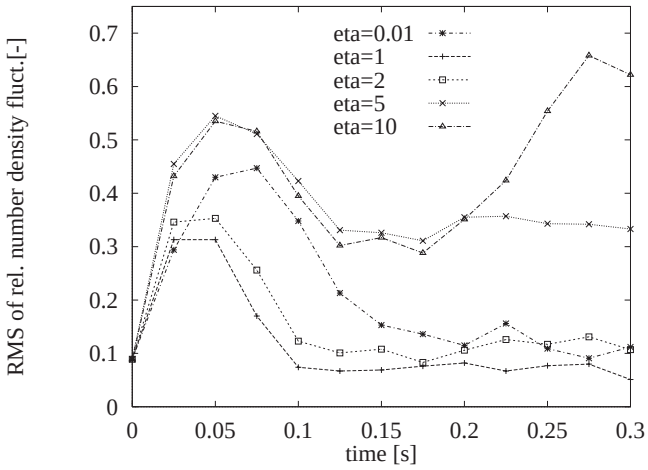

Fig. 12. RMS of relative number density fluctuation $n_{\text{fluct, RMS}}$.

For the dilute flow, the maximum of $n_{\text{fluct, RMS}}$ is reached at about $a = 0.075$ s. After that $n_{\text{fluct, RMS}}$ decreases down to the level of a homogeneous distribution, which is reached at about $t = 0.2$ s. In contrast to the dilute case for $\eta = 1$ and $\eta = 2$ the maximum of $n_{\text{fluct, RMS}}$ is lower and also the flow becomes homogeneous much quicker. Obviously in these cases, particle–particle collisions enhance dispersion. The collisions damp the development of in-homogeneities and enhance their dissolution. For $\eta = 5$ and $\eta = 10$, the initial increase in $n_{\text{fluct, RMS}}$ is stronger than in the other cases. Furthermore, after reaching its maximum at $t = 0.05$ s $n_{\text{fluct, RMS}}$ is only partly reduced. For $\eta = 5$, it remains almost constant on a higher level, whereas for $\eta = 10$, it even increases again for $t > 0.175$ s. In these two cases, inter-particle collisions enhance the development of an inhomogeneous concentration distribution and damp the dissolution of inhomogeneities.

5. Conclusion

Simulations of gas–solid flows in a horizontal channel were presented. The simulations were transient applying the Simulataneous Particle Tracking technique. Particle–particle collisions were accounted for using a stochastic model. Simulations were carried out for different particle loadings in order to examine the influence of loading and collisions on the motion of the particle phase. The change of gas flow properties due to the presence of particles was not considered.

Particle-particle collisions were found to have a significant effect on the particle concentration distribution in the channel. For particle to gas mass loading ratios of $\eta = 1$ and $\eta = 2$ collisions tended to enhance particle dispersion, whereas for higher loading ratios of $\eta = 5$ and $\eta = 10$, collisions enhanced the development of ''clusters'', i.e. local areas of higher particle concentration.

In the simulations presented in this paper, mass loading was the only variable parameter. Of course, there are many other physical and geometrical parameters that may influence the flow behaviour significantly, e.g. particle size and shape, gas velocity, channel size, phase coupling and so on. Hence, many more simulations as well as experimental investigations are required to understand the mechanisms of cluster formation and development.

Acknowledgements

The work presented in this paper was supported by the German Research Foundation (Deutsche Forschungsgemeinschaft—DFG) through the Collaborative Research Centre (Sonderforschungsbereich—SFB) 393. The simulations presented here were carried out on the Cray T3D at Edinburgh Parallel Computing Centre (EPCC), with support of the TRACS programme of the European Community.

References

Bird, G.A., 1976. Molecular Gas Dynamics. Oxford University Press, Oxford.
Bird, G.A., 1989. Perception of numerical methods in rarefied gas dynamics. Progr. Astro. and Aero 118, 211–226.
Bird, G.A., 1994. Molecular Gas Dynamics and the Direct Simulation of Gas Flows. Clarendon Press, Oxford.
Dennis, S.C.R., Singh, S.N., Ingham, D.B., 1980. The steady flow due to a rotating sphere at low and moderate Reynolds numbers. J. Fluid Mech. 101, 257–279.
Illner, R., Neunzert, H., 1987. On simulation methods for the Boltzmann equation. Transport Theory and Statistical Physics 16, 141–154.
Kitron, A., Elperin, T., Tamir, A., 1989. Monte Carlo analysis of wall erosion and direct contact heat transfer by impinging two-phase jets. J. Thermophysics 3, 112–122.
Kitron, A., Elperin, T., Tamir, A., 1990. Monte Carlo simulation of gas–solids suspension flows in impinging stream reactors. Int. J. Multiphase Flow 16, 1–17.
Milojevic, D., 1990. Lagrangian stochastic-deterministic (LSD) prediction of particle dispersion in turbulence. Particle and Particle Systems Characterization 7, 181–190.
Morsi, S.A., Alexander, A.J., 1972. An investigation of particle trajectories in two-phase flow systems. J. Fluid Mech. 55, 193–208.
Oesterlé, B., Petitjean, A., 1991. Simulation of particle-to-particle interactions in gas–solid flows. In: Proc. Int. Conf. on Multiphase Flows '91, Tsukuba, Japan, vol. 1, pp. 91–94.
Oesterlé, B., Petitjean, A., 1993. Simulation of particle-to-particle interactions in gas–solid flows. Int. J. Multiphase Flow 19, 199–211.
Sommerfeld, M., 1992. Modelling of particle-wall collisions in confined gas-particle flows. Int. J. Multiphase Flow 18, 905–926.
Tanaka, T., Kiribayashi, K., Tsuji, Y., 1991. Monte Carlo simulation of gas–solid flow in vertical pipe or channel. In: Proc. Int. Conf. on Multiphase Flows '91, Tsukuba, Japan, vol. 2, pp. 439–442.
Tanaka, T., Tsuji, Y., 1991. Numerical simulation of gas–solid two-phase flow in a vertical pipe: on the effect of inter-particle collision. In: ASME FED, Gas–Solid Flows, vol. 121, pp. 123–128 Book No. G00609.
Tsuji, Y., Morikawa, Y., Mizuno, O., 1985. Experimental measurement of the Magnus-force on a rotating sphere at low Reynolds numbers. Transactions of ASME, J. Fluids Eng. 107, 484–488.
Yonemura, S., Tanaka, T., Tsuji, Y., 1993. Cluster formation in gas–solid flow predicted by the DSMC method. In: ASME FED, Gas–Solid Flows, vol. 166, pp. 303–309 Book No.H00806.